



# Electrochemical removal of biofilms from titanium dental implant surfaces

Sebastian Schneider, Michael Rudolph, Vanessa Bause, Andreas Terfort \*

Institute of Inorganic and Analytical Chemistry, Goethe-University, Max-von-Laue-Str. 7, D-60438 Frankfurt am Main, Germany

## ARTICLE INFO

### Article history:

Received 16 September 2017

Received in revised form 15 January 2018

Accepted 15 January 2018

Available online xxxx

### Keywords:

Disinfection

*In situ* cleaning

Cell viability

Electrolysis

Gas evolution

Iodide

## ABSTRACT

The infection of dental implants may cause severe inflammation of tissue and even bone degradation if not treated. For titanium implants, a new, minimally invasive approach is the electrochemical removal of the biofilms including the disinfection of the metal surface. In this project, several parameters, such as electrode potentials and electrolyte compositions, were varied to understand the underlying mechanisms. Optimal electrolytes contained iodide as well as lactic acid. Electrochemical experiments, such as cyclic voltammetry or measurements of open circuit potentials, were performed in different cell set-ups to distinguish between different possible reactions. At the applied potentials of  $E < -1.4$  V, the hydrogen evolution reaction dominated at the implant surface, effectively lifting off the bacterial films. In addition, several disinfecting species are formed at the anode, such as triiodide and hydrogen peroxide. *Ex situ* tests with model biofilms of *E. coli* clearly demonstrated the effectiveness of the respective anolytes in killing the bacteria, as determined by the LIVE/DEAD™ assay. Using optimized electrolysis parameters of 30 s at 7.0 V and 300 mA, a 14-day old wildtype biofilm could be completely removed from dental implants *in vitro*.

© 2018 Elsevier B.V. All rights reserved.

## 1. Introduction

The success of dental implants as replacement for missing teeth is lowered by the complications of peri-implant mucositis and peri-implantitis [1,2]. Mucositis is defined as the reversible inflammation of soft tissue surrounding dental implants, whereas peri-implantitis is often described as irreversible inflammatory process that degenerates connective tissue between bone and osseointegrated oral implants and is often followed by the resorption of surrounding bone. Such severe complications are caused by the colonization of different pathogenic bacteria on the implant surface and their organization in bacterial biofilms. In case of medical malpractice or omitted treatment peri-implantitis can lead to complete disintegration of the implant [3,4]. Recent methods to treat peri-implantitis [5,6,7] include mechanical decontamination and local antiseptic or antibiotic treatment. Implant surface treatments are scaling, laser decontamination and photo-dynamic therapy, powder-blasting with biocompatible abrasives, chlorhexidine or hydrogen peroxide irrigation, or local application of antibiotics [5,6,7]. Most of these debridement protocols for dental implants have been derived from periodontology.

A novel, minimally invasive approach [8,9,10] to remove and disinfect dental implants utilizes the fact that titanium is an electrically conducting metal and the number of adherent microorganisms on dental implants could be drastically reduced by electrolysis [11,12,13]. In numerous case studies to verify the mode of action [14,15], the use of chlorhexidine [16,17], citric acid [18], hydrogen peroxide [18], iodine compounds [19,20,21,22], variation of the pH value [23], gas bubbles [24], powder-blasting and mechanical debridement [25,26] to remove biofilms from implant surfaces, were investigated. Chemical disinfectants [27,28] or antibiotics affect mainly the permeation properties of the cytoplasmic and external membranes of bacteria, e.g. by interactions with phospholipids or by denaturation of specific proteins, by oxidation of peptide links and structurally important compounds and, in the case of iodine compounds, by blocking electron transport through electrophilic reactions with enzymes of the respiratory chain of aerobic microorganisms [15]. The *in situ* generation of disinfectants is well-known for water disinfection [29,30,31] and was successfully transferred to dental implant purification in recent proof-of-concept studies [11–13,28,32–45] and by exploitation of the bioelectrical effect [46,47,48]. Electrochemical treatment of dental implants combines the antibacterial efficacy of bactericides, but with low free concentration of toxic substances as they are only generated during electrolysis, with the direct oxidation of bacterial enzymes and proteins. Especially results from D. Ren et al. [49,50] demonstrated that pathogenic bacteria such as *Streptococcus mutans*, *Staphylococcus aureus* and *Pseudomonas*

\* Corresponding author at: Max-von-Laue-Str. 7, D-60438 Frankfurt am Main, Germany.

E-mail address: [aterfort@chemie.uni-frankfurt.de](mailto:aterfort@chemie.uni-frankfurt.de) (A. Terfort).

*aeruginosa* could be efficiently killed by low level direct current treatment and/or in combination with antibiotics.

In this work we investigate the beneficial effect of electrochemical removal of *E. coli* biofilms by the hydrogen evolution reaction (HER) at titanium surfaces in combination with the *in situ* generation of a disinfecting agent. Stable and effective electrolysis parameters that fulfill typical application specifications were identified [8,9,10]. The electrolysis products were analyzed and quantified if applicable. The electrochemistry of bare titanium surfaces in the used electrolytes was investigated by cyclic voltammetry (CV), electrochemical impedance spectroscopy (EIS) and monitoring of the open circuit potential,  $E_{OC}$ , before and the open cell voltage,  $E_{CV}$ , during electrolysis. In order to test the disinfecting efficacy of the method, *E. coli* biofilms were grown on different titanium surfaces and their removal under various conditions was tested by the LIVE/DEAD™ assay via fluorescence microscopy and monitored by infrared absorption-reflection spectroscopy (IRRAS). The morphologies of bare and modified titanium surfaces were assessed with atomic force microscopy (AFM) and scanning electron microscopy (SEM). Finally the developed method was used to remove a mature wildtype biofilm completely from a commercial dental implant.

## 2. Materials and methods

### 2.1. Chemicals and electrolytes

All chemicals were of analytical/Ph. Eur. grade and were used as received (Sigma Aldrich, Merck, Alfa Aesar). Table 1 shows the concentration levels of electrolytes that were used. All solutions were prepared from MilliQ water (Millipore) in measuring flasks.

### 2.2. Substrate preparation

Titanium substrates were fabricated using a conventional multi-pocket electron beam evaporation chamber (Pfeiffer Vacuum 50 Classic) with a quartz crystal microbalance (QCM) thickness monitor and Meissner cooling trap. Si(100) wafers (Active Business Company) were placed on the sample holder disc and mounted 20 cm above the source at the same level as the QCM element. Evaporation was conducted at pressures below  $10^{-5}$  hPa, while the sample holder was rotated. A layer of 50 nm of titanium (99.999%, Alfa Aesar) was evaporated with a rate of 0.5 Å/s onto the wafers. Substrates were removed after allowing the system to cool down to ambient temperature and cut into  $10 \times 10$  mm<sup>2</sup>. For surface modification the substrates were stirred in concentrated HCl at RT overnight.

**Table 1**

Concentration levels of the investigated electrolytes; final volume 100.00 mL. KI – potassium iodide, LA – D/L lactic acid.

Solution	Chemicals	M/g mol <sup>-1</sup>	m/g	n/mmol	c/mmol L <sup>-1</sup>
A	Potassium iodide (KI)	166.00	12.5	75.4	754
A*	KI	166.00	12.5	75.4	754
	D/L Lactic acid (LA)	90.08	0.57	6.3	63
B	KI	166.00	6.26	37.7	377
B*	KI	166.00	6.26	37.7	377
	LA	90.08	0.29	3.2	32
C	KI	166.00	12.5	75.4	754
	L-Malic acid	134.09	0.58	4.3	43
D	KI	166.00	12.5	75.4	754
	Ascorbic acid	176.13	0.86	4.9	49
E	KI	166.00	12.5	75.4	754
	Citric acid	192.13	1.21	6.3	63
F	Sodium formate	68.01	25.0	368	$3.68 \cdot 10^3$
	LA	90.08	1.26	13.9	139
G	Sodium acetate	82.03	25.0	305	$3.05 \cdot 10^3$
	LA	90.08	1.26	13.9	139

### 2.3. Surface morphology characterization

Samples for AFM and SEM were immersed in 25% glutaraldehyde overnight, afterwards dipped ten times in 50% EtOH [51] and dried in a vacuum desiccator for at least 2 h. Surface topography was acquired on an atomic force microscope NT-MDT Solver Pro (NT-MDT) in semi-contact mode with a silicon tip (HA\_NC Etalon, spring constant 3.5 N/m) and at different scanning areas at a scan rate of 1 Hz. The experiments were conducted in air and at room temperature. Calibration and testing of tip quality was achieved after each run by comparison with TGS1 and TGT1 test patterns (NT-MDT). Morphology of the samples was studied using a high-resolution scanning electron microscope (Atomica Amray 1920ECO) at an acceleration voltage of 10–15 kV. Samples were sputtered with ~10 nm of gold when necessary (Edwards Sputter Coater).

### 2.4. Infrared reflection-absorption spectroscopy

Acquisition of IR spectra of biofilms on Ti substrates was performed with a Thermo Fisher Scientific Nicolet 6700 FT-IR spectrometer (HeNe laser,  $\lambda$ : 632.8 nm; IRRAS unit SmartSAGA, using *p*-polarized IR radiation, incidence angle of 80° relative to the sample surface normal) with a LN-cooled mercury-cadmium-telluride detector. The beam path of the spectrometer was purged with dried and CO<sub>2</sub>-free air. For each spectrum at least  $4 \times 256$  scans were recorded from 650 cm<sup>-1</sup> to 4000 cm<sup>-1</sup> with a resolution of 4 cm<sup>-1</sup>, followed by a baseline correction and averaging afterwards. Background was a blank substrate. The spectra were evaluated with the Thermo Fisher Omnic software (version 8.0.380).

### 2.5. Electrolysis set-up and cell voltage

For electrolysis four custom-built cells were used, shown in Fig. S1. Tests were conducted in all cell types. The electrodes for electrolysis were a titanium dental implant (Straumann BL Ø 4.1 mm, RC SLA™, Grade 4, L: 11 mm), custom-built titanium disc electrodes (Ø 3 mm) or freshly prepared titanium substrates as cathode and a platinized titanium rod (Custom-built, Ø 4.0 mm, L: 10 mm) and Pt coils as anode. Voltage was applied by a laboratory power supply (VotcraftPlus VSP1410HE) and the circuit inputs were checked before electrolysis with a digital high precision multimeter (Fluke 87 True RMS). Standard conditions were 7 V for 30 s with a current of 300 mA over a junction between the titanium cathode and a platinized titanium anode (cell type “Vert”). The electrolyses in cell types “Hor” and “HorSep” were conducted at 37.0 °C unless stated otherwise. Temperature was controlled by a Julabo FP40 thermostat with a Julabo HD controller. Cell contents were homogenized after electrolysis; 5.00 mL per test were sampled and stored in the dark at 4 °C. Each sampling point was tested three times. The investigated electrolysis times were 10, 20, 30, 60 and 300 s at 300 mA. Open circuit potential as well as current measurements during electrolysis were performed with Pt coil, Pt disc (Ø 3 mm) and Pt wire electrodes and a Vertex Potentiostat (Ivium Technologies) controlled with the IviumSoft software (Version 2.587). Applied cell voltages were 1, 3, 5, 7, 9 and 11 V and the measured potentials were recorded with the subprogram  $E_{oc}$  monitor (interval: 0.1 s, run time: 150/300 s, eq. time: 20 s, potential range: 10 V). Electrolysis current was monitored with the subprogram for amperometric detection ( $E_{start}$  = 0.00 V, interval time: 0.5 s, N samples: 300 pnts, eq. time: 20 s, current range: 1 A).

### 2.6. Electrochemistry

CV and EIS measurements were performed in custom-built three-electrode electrochemical cell setups mentioned above using a Vertex potentiostat (Ivium Technologies). Data acquisition and evaluation were performed using IviumSoft (Version 2.587). The measurements

were performed at room temperature. If the electrolytes were degassed (mentioned in the text), a stream of Ar was passed at least for 30 min through the solutions. The counter electrode was a coiled platinum wire and the pseudo reference electrode was an Ag wire ( $E_{\text{Ag}/\text{Ag}^+} = 0.023 \text{ V vs. Ag/AgCl}$ , 3 M NaCl, ALS Electrochemistry). The stability of this pseudo reference electrode is demonstrated in Fig. S2. Cylindrical PDMS cells (poly(dimethylsiloxane), Sylgard 184, Dow Corning; inner diameter: 5 mm, inner height: 5 mm,  $A_{\text{geo}}: 0.196 \text{ cm}^2$ ) were used after 24 h of Soxhlet extraction with ethanol. Titanium substrates were used as working electrodes. For comparison specifically fabricated titanium disc electrodes ( $\varnothing$  3 mm, PVDF isolation) with/without sandblasted, acid-etched (SLA) surface finishing were also tested as working electrodes.

## 2.7. Bacterial cultures and biofilm growth

Non-fimbriated *E. coli* K12 bacteria (JM101) [52] and *E. coli*-GFP (HB101) [53] were purchased from New England BioLabs Inc. and used as received. Small aliquots of bacteria (test cultures stored at  $-80^\circ\text{C}$ ) were cultured in a 50 mL Falcon tube that contained 20 mL lysogeny broth (LB) [54] growth medium and in the case of *E. coli*-GFP the strain-specific antibiotics, adjusted with phosphate buffer solution (PBS, pH 7.6). The solution was incubated for 16 h at  $37^\circ\text{C}$  and 100 rpm until the exponential growth phase was reached ( $\text{OD}_{600} = 0.5$ – $1.5$ , checked every 4 h). These bacterial suspensions (“overnight culture”) were used directly to graft biofilms onto titanium samples. All of the samples (titanium thin film substrates and disc electrodes) were heated up to  $80^\circ\text{C}$  for 20 min to sanitize the surfaces. The substrate samples,  $10 \times 10 \text{ mm}^2$ , were placed in sterile 12-well plates (Sarstedt), completely covered with 2.0 mL of LB medium and 200  $\mu\text{L}$  of the overnight culture ( $\text{OD}_{600}$  0.5) and shaken at  $37^\circ\text{C}$  and 100 rpm for 24 h. Titanium disc electrodes were positioned in 20 mL Falcon tubes, 5 mL LB medium and 500  $\mu\text{L}$  overnight culture were added. These samples were shaken at  $37^\circ\text{C}$  and 100 rpm for 48 h.

Growth protocol for the wild type biofilm: 10 saliva samples were obtained (5 male, 5 female test subjects), mixed and cultivated in a nutrition medium for 24 h [65]. From this culture 1.5 mL were placed together with dental implant screws into Falcon tubes, filled up with fresh growth medium and biofilms were grown at  $37^\circ\text{C}$  for 48 h, before the growth medium was exchanged. This procedure was repeated for 14 days.

## 2.8. Viability assay

After a growth period of 24–48 h the samples were dipped ten times in freshly prepared PBS solution to wash off non-adherent bacteria. Thereafter the samples were either tested directly or were incubated in the respective agent/electrolyte for another 12 h before testing. For this, the titanium samples were then immersed in PBS solution and stained with a 1:1 mixture of SYTO<sup>TM</sup> 9 and propidium iodide (PI) solutions (BacLight<sup>TM</sup> cell viability kit, Thermo Fisher L7012) according to supplier instructions. Afterwards the substrates were immediately transferred to an epifluorescence microscope (Olympus BX51, Infinity 3 Analyzer, software Infinity Analyze 5.0) equipped with a metal halide lamp, a 488 nm band filter for excitation, a 500 nm edge filter for SYTO<sup>TM</sup> 9 and a 620 nm edge filter for PI detection and then the number of adherent bacteria was counted. To limit the viability analysis to fluorescent *E. coli* and to eliminate bias in the data analysis based on fluorescence intensity, a normalization of the gamma value was performed, before a threshold was put onto the respective color channel (red/green) to generate a binary image. These images were segmented and the surface-adherent bacteria were counted automatically using the Fiji ImageJ (Version 1.51 g) package [55].

## 2.9. High-speed video recording

A Canon CMOS/DIGIC4-RGB digital camera (Powershot SX220HS, Canon Deutschland GmbH, Krefeld) was connected to a MSZ 5600 stereo microscope (A. Krüss Optronik GmbH, Hamburg). The recording setup is sketched in Fig. S3. Images of the electrolysis reaction at a bare titanium dental implant and of the removal of a matured wild type multi-species biofilm were captured at a rate of 240 images per second. The size information on gas bubbles was determined by evaluating the bubble sizes in singular high speed video photographs and comparing it to the known diameter of the implant in the same photograph. The average bubble diameter was gained by the sum of all found diameters divided by the number of counted bubbles in the specific photograph at a given point of time in the experiment.

## 2.10. Analysis of the electrolytes before and after electrolysis

The electrolytic solutions (catholyte, anolyte) were analyzed for pH, ozone, hydrogen peroxide, iodine, organic reaction products and reactive halogenides before and after electrolysis by pH meter, photometric methods, ion chromatography and gas chromatography/mass spectrometry. The experimental details can be found in the supporting information.

## 3. Results and discussion

### 3.1. Literature known electrode reactions

Electrolysis as a means for disinfection is advantageous, because it permits the localized generation of active substances, the nature of which in turn depends on the applied potential and current density. Particularly the electrolysis of aqueous solutions is well-known [29,31]: Water is decomposed at the cathode to  $\text{H}_2$  and  $\text{OH}^-$  [56,57] and at the anode  $\text{O}_2$  and  $\text{H}^+$  are generated (eq. (C1) and (A1)).

When other species, e.g. iodide and LA, are present, highly reactive species [11,33,34,43] such as  $\text{I}_2$ , HOI [58,59],  $\text{H}_2\text{O}_2$  [60], ozone and hydroxyl radicals could be generated (eq. (C4)–(C8) as well as (A2)–(A9) and (A15)). The electrochemical formation of such important disinfectants depends mainly on the applied current/voltage and on the quality, composition and surface properties of the electrode material [30]. Oxidative side reactions of inorganic ((A10), (A11)) [61] and organic ((A12), (A13)) electrolyte components are possible. For example LA and generated iodine may undergo haloform reactions [62] (A13) in alkaline environment, esterification [63,64] or other iodine-mediated organic reactions [65].

### 3.2. Electrolysis at pure titanium electrodes and characterization of such surfaces

Bare titanium electrodes and substrates were characterized by SEM, AFM, IRRAS and electroanalytical techniques like measurement of open circuit potential ( $E_{\text{OCP}}$ ) and cell voltage ( $E_{\text{CVE}}$ ) during electrolysis, CV and EIS.

For electrochemical and microbiological studies titanium substrates with a roughness ( $S_a$ ) of 0.5 nm were fabricated (Fig. 1a). To compare the results with those of a SLA type dental implant surface, a small number of substrates were successfully etched with concentrated hydrochloric acid (7 mol/L) for 24 h (Fig. 1b). The roughness  $S_a$  of these substrates was significantly increased to 4.6 nm. As titanium films with native oxide layers show excellent reflectivity for infrared light as known from literature [66], IRRAS measurements could be performed to characterize the adsorbates. Clean titanium substrates turned out to be ideal background samples for the measurements with adherent biofilms.

It is known from literature [67] that factors including surface charge and surface energy, roughness and topography of the given implant



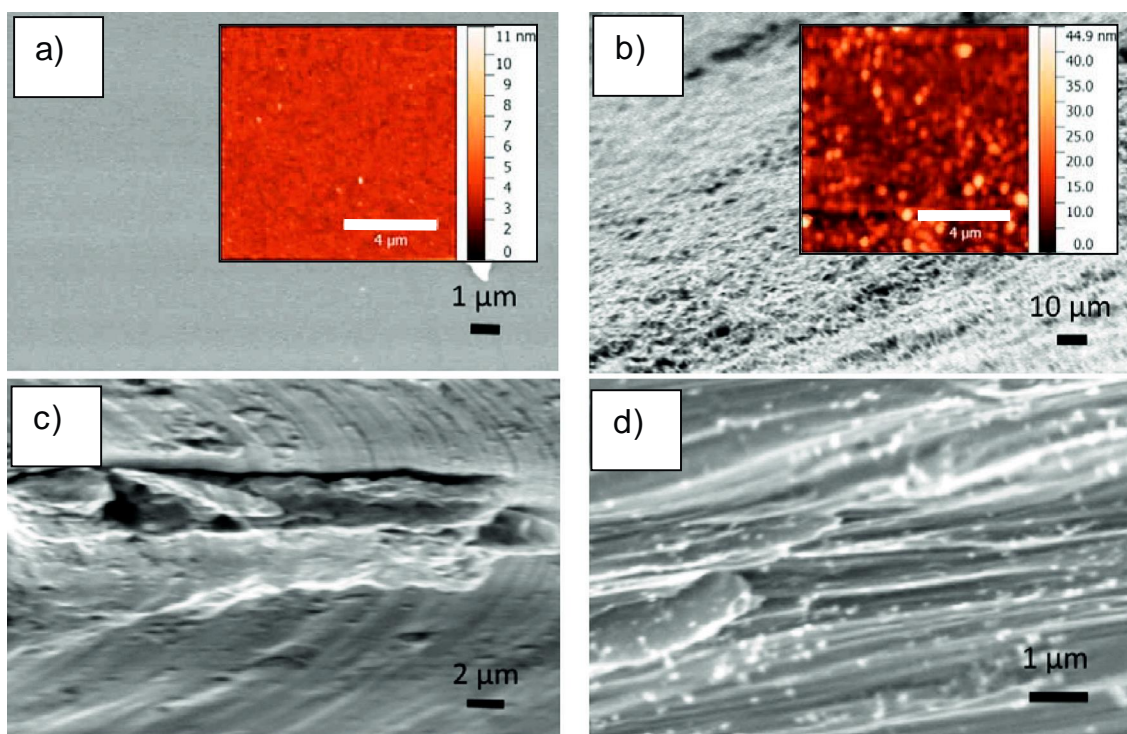


**Fig. 1.** SEM images of bare titanium substrates (a, inset: AFM image), acid-etched titanium substrate (b, inset: AFM image), titanium disc electrode before (c) and after electrolysis (d) in A\* for 30 s at 7 V and 300 mA.

surface play a vital role in the bacterial adhesion process. Thus the above mentioned material properties of the given titanium substrate or implant will determine how biofilm forming bacteria will adhere to such surfaces. In our study we tried to minimize the differences of titanium thin films and implant bulk material in microstructure, crystalline orientation and nature of the oxide films as well as hydrogen charging by the appropriate preparation method. Further investigations are needed to fully understand the influence of these material properties on bacterial adhesion processes.

Starting from literature values [8,9,10] we optimized the electrolysis conditions, details on this optimization will be reported elsewhere. Electrolysis in undivided cells (types “Vert”, “Hor” and “Sub”) was generally conducted by application of an external voltage of 7 V for 30 s (typical current: 300 mA) between a titanium cathode (dental implant, disc electrode or substrate) and a platinum anode. For electrolyses in cell type “HorSep” the observed conditions were approximately 2 V, 30 s where the sintered glass diaphragm and the large distance between both electrodes led to a reduction of applied potential. The investigation of electrode reactions was primarily conducted with titanium disc electrodes, where insulating nanoparticulate residues were observed after electrolysis in A\* (Fig. 1c and d). We assume that these particles consist of poly(lactic acid), which has been formed by radical or ionic chain growth polymerization (polycondensation) due to the redox chemistry at the cathode. This residue was not analyzed further.

The monitoring of the electrolyses was accomplished by simultaneous measurement of the cell voltage ( $E_{C/E}$ ) with two separate platinum electrodes (Fig. 2a) while the working electrode was polarized to electrolysis potentials. Exemplarily an  $E_{C/E}$  measurement in cell types “Vert” and “HorSep” (Fig. 2b) as well as the corresponding photographs at the specific moments during the electrolysis are shown in Fig. 2c. From the beginning of the electrolysis a vigorous gas evolution was observed at the cathode in all electrolytes. The formed gas was hydrogen as tested by mass spectrometry and Knallgas test. The detachment of hydrogen bubbles was observed as a massive drop in  $E_{C/E}$  followed by

a steep rise to the former potential level (Fig. 2b, phase II, grey box, indicated by an arrow in Fig. 2c). Overall the potential curve decayed after such bubble detachment events to a gas film/solution equilibrium until the cathode surface was completely occupied by gas molecules (Fig. 2b,c, phase II to III). During this period a reddish, brown precipitate was formed at the anode that dissolved immediately after formation (phase III, yellow box in Fig. 2b). By CV and spectrophotometry of the electrolyte afterwards, it could be demonstrated that iodine/triiodide respectively polyiodide was formed [69,70,71,72]. When chunks of the polyiodide separated from the electrode surface (pink box in Fig. 2b, chunks indicated by an arrow in phase IV in Fig. 2c), the recorded potential increased as fresh iodide ions diffused towards the now temporarily available anode surface and further oxidation reactions occurred. After the electrolysis was terminated, the potential obeyed an exponential decay law with  $\tau = (14 \pm 4)$  s until the OCP value before electrolysis was reached again (Fig. 2b,c, phase V to VI, red solid line) correlated to the diffusion of formed species along the concentration gradient from one electrode to the other.

To gain deeper insight into the HER at the dental implant cathode surface high-speed video analysis of the electrolysis was performed. From single photographs it was evident that the HER starts preferentially on the edges of the thread of the implant screw (Fig. S4). For the grooves less reactivity was observed. The formed gas bubbles increase in average size from a diameter of initially 270  $\mu\text{m}$  to 515  $\mu\text{m}$  after 30 s of electrolysis and detached from the implant surface at various moments and with statistically distributed dimensions.

### 3.3. Electrode reactions at titanium cathodes

The main competing reactions at such titanium cathodes in aqueous solutions are the hydrogen evolution reaction (HER, (C1)) [73,74] and the rather sluggish oxygen reduction reaction (ORR, (C2)–(C8)) [54,75–83]. The latter can be understood by the four electron pathway



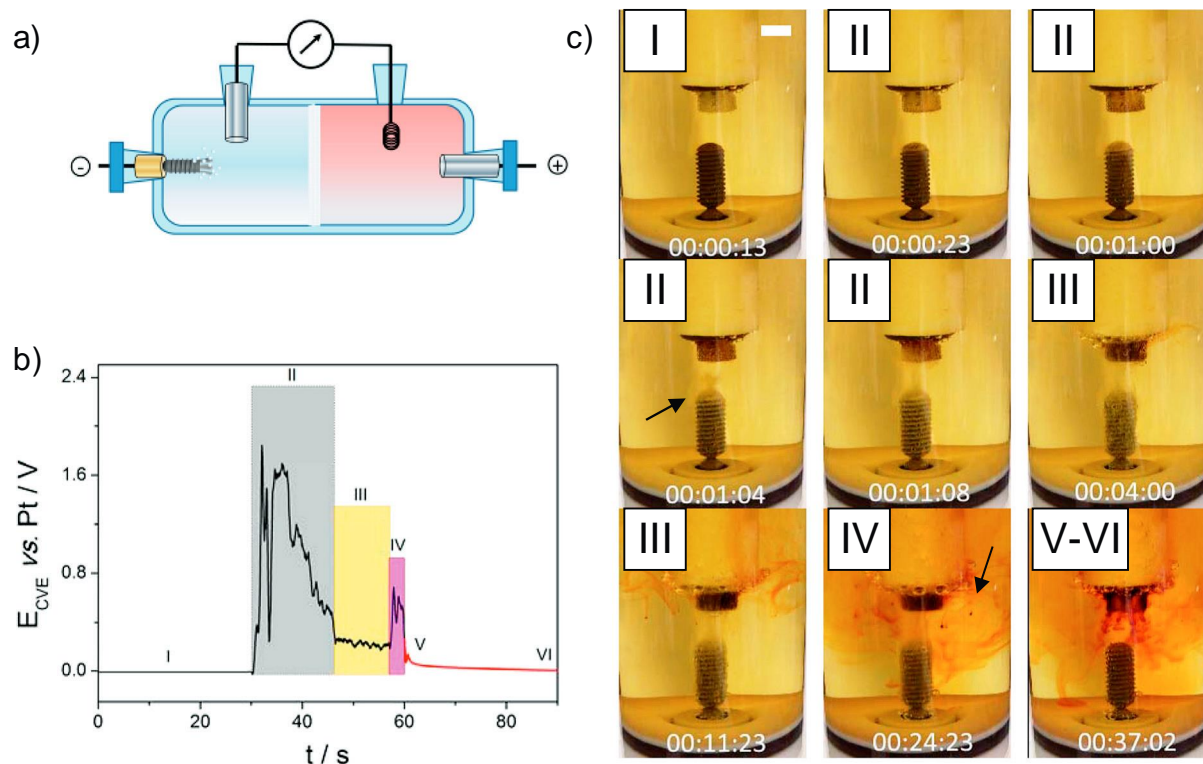


**Fig. 2.** a) Schematic representation of the electrolysis cell “HorSep” with titanium test specimen (left) and Pt anode (right), two Pt electrodes for measurement of  $E_{C_{VE}}$ ; b) Cell voltage measurement during electrolysis in A\*, cell type “HorSep”, 37 °C, time program: 30 s OCP, 30 s electrolysis at 11 V, 30 s rest to OCP. The monitored phases are: I) cell in equilibrium state, II) massive hydrogen evolution at the cathode with voltage spikes during gas bubble separation, III) polyiodide formation phase, cell voltage nearly constant, IV) separation of polyiodide chunks, V) voltage drop according to diffusional exponential decay of current, VI) cell in new equilibrium state; c) Corresponding photographs of the electrolysis in cell type “Vert”. When the reaction is stopped after 30 s, the gas evolution drops and the reaction products at the anode diffuse rapidly to the cathode (V–VI). Scale bar (shown in photograph I): 4 mm.

in alkaline media according to Parkinson et al. [84] and Clark et al. [85] or by the two electron pathway in neutral and acidic solutions, including the generation of hydrogen peroxide ((C6), (C7)), published by Clechet et al. [86]. Starting from the known ORR signal at  $-1.45$  V vs. Ag/AgCl (Fig. 3a), easily obtained in  $O_2$ -saturated 0.1 M tetra *n* butyl ammonium hexafluorophosphate (TBAHFP) solution in DCM on platinum working electrodes and in good agreement with reported values [87], we tested titanium substrates and disc electrodes for the ORR.

In solution A (Fig. 3b,c) we observed the ORR signal at  $-0.75$  V vs. Ag/Ag<sup>+</sup> that corresponded fairly to known values at pH 5–6 [54]. When LA was present the signal was broadened and due to the lower pH value the ORR onset was shifted to more anodic potentials (Fig. 3d), starting at  $-0.60$  V vs. Ag/Ag<sup>+</sup> [54]. On the contrary, the HER was shifted to cathodic potentials with LA containing electrolytes (Fig. 3d), which was also expected from literature [54,70,71] because of the lowering of the pH value and influencing the local oxide environment. Torresi et al. [71] attributed shifts of the HER on titanium/titanium dioxide film electrodes to two processes that simultaneously take place: i) the film dissolution by reduction of TiO<sub>2</sub> oxide films to oxy-hydroxy species of Ti(III), ii) the film loading with hydrogen species. Observed shifts occur without changes of the kinetics of the HER but with an increase of “specific activity” of the surface (either by titanium hydride formation or hydrogen absorption in the oxide [71]). Therefore we conclude that the HER in electrolytes containing KI and LA starts at  $-1.4$  V (degassed) to  $-1.05$  V (ambient or  $O_2$  saturated) vs. Ag/Ag<sup>+</sup> and depends on the surface composition and preferred adherents on the native titanium oxide film. As in pure KI electrolytes, no shift of the HER was recognized (Fig. 3c), the change in potential onset must be due to the presence of LA. As already mentioned, the variation of the pH at the

electrode could be responsible for this [54,70,71]. So at electrolysis potentials below  $-1.4$  V vs. Ag/Ag<sup>+</sup>, i.e. absolute voltages larger than 1.4 V at the cathode, the ORR occurs besides the HER at titanium dental implants, but with slower kinetics [54].

### 3.4. Disinfection impact of electrolyte components or electrolyzed electrolytes

In this study a common approach to generate disinfectants was adapted [11,29,30,31] to kill bacteria adhering to dental implant surfaces. At the cathode hydrogen is formed and in unbuffered solutions, the pH will rise due to the formation of hydroxide ions. So the electrolysis of aqueous solutions relates to a change of pH value. Therefore quantitative pH measurements with a pH-sensitive electrode revealed a drastic increase of pH at the cathode after electrolysis of KI solutions A and B (Table 3), which was expected by equations (C1), (C2), (C7) and (C8) (Table 2). At the anode no gas evolution was observed during the electrolysis and the pH value remained on the same level afterwards, i.e. reactions (A1), (A6), (A7), (A9), (A10), (A11), (A13) and (A15) (Table 2) are rather unlikely – especially the oxygen evolution overpotential was not reached, so A1 might be excluded. When  $\alpha$ -hydroxycarboxylic acids were present (A\*, B\*, C, D) the pH of the electrolyte was buffered in the acidic region at the cathode as well as at the anode. The reactions (C3) and (C4) (Table 2) may be favored at low pH. Hydrogen peroxide formed only at the anode. When LA was present, the testing method yielded false positive results by reaction of the LA and of the formed iodine with the indicative reagent dye (blind test not shown).

It is known from literature [88] that the formation of ozone must be detected at lower temperature due to the decreased stability of ozone at

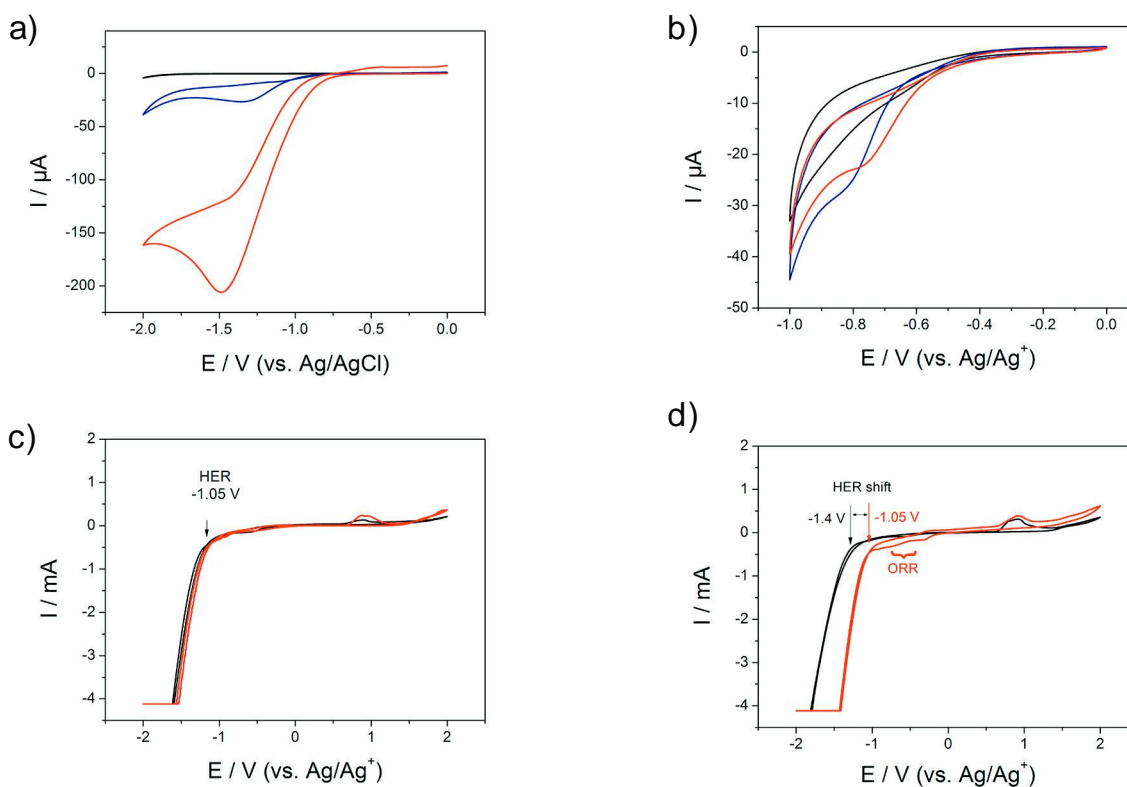


**Fig. 3.** a) Oxygen reduction reaction (ORR) in 0.1 M Bu<sub>4</sub>NPF<sub>6</sub> in Ar-purged (black), ambient (blue) and O<sub>2</sub>-purged dichloromethane (red), Pt-WE, Pt-CE, RE: Ag/AgCl,  $\nu = 100$  mV/s, 5th cycle; b) ORR in Ar-purged (black), ambient (blue) and O<sub>2</sub>-purged solutions (red) of A at Ti-WE, Pt-CE, Ag-RE,  $\nu = 25$  mV/s, 5th cycle. Hydrogen evolution reaction (HER) at titanium electrodes in 754 mM KI electrolytes without (c) and with 63 mM lactic acid (d). CV measurements of Ar-purged (black) and O<sub>2</sub>-purged solutions (red); WE: Ti, CE: Pt, RE: Ag,  $\nu = 100$  mV/s, 5th cycle. (For interpretation of the references to color in this figure legend, the reader is referred to the web version of this article.)

elevated temperatures (Table 2). Therefore the electrolyses were conducted at 4 °C and the reagents, washing solutions and the cuvettes were cooled to 4 °C. The complete analysis was conducted at low temperature and electrolyzed samples were transferred immediately to the temperature-controlled measurement set-up. For the investigated electrolytes after 30 s of electrolysis, the found ozone quantities were below the limit of detection (LOD) of 6 μg/L.

Ion chromatography results for the electrolytes A and A\* are shown in Fig. S5. In the case of a pure KI solution the major product was

triiodide formed by the generation of I<sub>2</sub> and indicated by a retention time shift due to an increase of the m/z ratio of the specific ion. Another peak at  $t_R = 4.88$  min was attributed to naturally occurring iodine species such as OI<sup>−</sup> and IO<sub>3</sub><sup>−</sup> in aqueous solutions in the specific pH region [59,89,90]. For A\* it was found that the concentration of LA after the electrolysis did not change significantly. The chromatograms for the electrolyzed samples further revealed no additional ionic compounds. The analysis of organic iodine species of electrolyzed samples of A\* by gas chromatography coupled to mass spectrometry (GC-MS) showed

**Table 2**

Probable electrode reactions in aqueous solutions that contain iodide and lactic acid or other α-hydroxycarboxylic acids as found in literature [11,29,31,54–58,60–63].

Reactions at cathode		Reactions at anode	
(C1)	$2 \text{H}_2\text{O} + 2 \text{e}^- \rightarrow \text{H}_2 + 2 \text{OH}^-$	(A1)	$2 \text{H}_2\text{O} \rightarrow \text{O}_2 + 4 \text{H}^+ + 4 \text{e}^-$
(C2)	$\text{O}_2 + 4 \text{e}^- + 2 \text{H}_2\text{O} \rightarrow 4 \text{OH}^-$	(A2)	$2 \text{I}^- \rightarrow \text{I}_2 + 2 \text{e}^-$
(C3)	$\text{O}_2 + 4 \text{H}^+ + 4 \text{e}^- \rightarrow 2 \text{H}_2\text{O}$	(A3)	$\text{I}_2 + \text{I}^- \rightarrow \text{I}_3^-$
(C4)	$\text{O}_2 + 2 \text{H}^+ + 2 \text{e}^- \rightarrow \text{H}_2\text{O}_2$	(A4)	$2 \text{I}^- \rightarrow 2 \text{I}^\bullet + 2 \text{e}^-$
(C5)	$\text{O}_2 + \text{e}^- + \text{H}_2\text{O} \rightarrow \text{OH}^- + \text{HO}_2^\bullet$	(A5)	$2 \text{I}^\bullet \rightarrow \text{I}_2$
(C6)	$\text{HO}_2^\bullet + 2 \text{H}_2\text{O} \rightarrow \text{OH}^\bullet + \text{H}_2\text{O}_2$	(A6)	$\text{I}^\bullet + \text{H}_2\text{O} \rightarrow \text{I}^- + \text{OH}^\bullet + \text{H}^+$
(C7)	$\text{H}_2\text{O}_2 + \text{e}^- \rightarrow \text{OH}^\bullet + \text{OH}^-$	(A7)	$\text{H}_2\text{O} \rightarrow \text{OH}^\bullet + \text{H}^+ + \text{e}^-$
(C8)	$\text{OH}^\bullet + \text{e}^- \rightarrow \text{OH}^-$	(A8)	$2 \text{OH}^\bullet \rightarrow \text{H}_2\text{O}_2$
		(A9)	$\text{I}_2 + \text{H}_2\text{O} \rightarrow \text{HOI} + \text{H}^+ + \text{I}^-$
		(A10)	$3 \text{I}_2 + 3 \text{H}_2\text{O} \rightarrow \text{IO}_3^- + 5 \text{I}^- + 6 \text{H}^+$
		(A11)	$\text{IO}_3^- + \text{I}^- + 6 \text{H}^+ \rightarrow \text{I}_2 + 3 \text{H}_2\text{O}$
		(A12)	$2 \text{R-COOH} + 2 \text{I}^- \rightarrow 2 \text{R-COO}^- + \text{I}_2 + \text{H}_2$
		(A13)	$\text{I}_2 + 2 \text{OH}^- \rightarrow \text{I}^- + \text{IO}^- + \text{H}_2\text{O}$
			$(\text{H}_3\text{C})\text{R}'\text{CH-OH} + \text{IO}^- \rightarrow (\text{H}_3\text{C})\text{R}'\text{C=O} + \text{I}^- + \text{H}_2\text{O}$
			$(\text{H}_3\text{C})\text{R}'\text{C=O} + 2 \text{I}_2 + 2 \text{OH}^- \rightarrow$
			$\text{HCl}_3 + \text{R}'\text{COO}^- + 2 \text{H}_2\text{O} + \text{I}^-$
		(A14)	$\text{R-COO}^- \rightarrow \text{R}^\bullet + \text{CO}_2 + \text{e}^-$
		(A15)	$\text{O}_2 + \text{H}_2\text{O} \rightarrow \text{O}_3 + 2 \text{H}^+ + 2 \text{e}^-$

**Table 3**

Analytical data on electrolytes after electrolysis in “HorSep” (37.0 °C, 7 V, 30 s, 300 mA); An – anolyte, Cat – catholyte, RX – reactive halogene species ( $\text{IO}_3^-$ , HOI,  $\text{I}^-$ ; LOQ: 35 ppm). Values in parentheses are before electrolysis. Found concentrations of ozone, hydrogen peroxide, iodine and reactive halogenides in parts per million [ppm]. Ozone concentration was determined at 4 °C, LOD: 6  $\mu\text{g/L}$  [85].

#	pH		$\text{O}_3/\text{ppm}$		$\text{H}_2\text{O}_2/\text{ppm}$		$\text{I}_2/\text{g L}^{-1}$	RX/ppm	
	An	Cat	An	Cat	An	Cat	Bulk	An	Cat
A	6.25 (6.10)	11.10 (6.30)	<LOD	<LOD	25	0	13	99	<LOQ
A*	2.18 (2.20)	2.31 (2.29)	<LOD	<LOD	>25	>25	10	288	63
B	6.46 (6.38)	11.06 (6.50)	<LOD	<LOD	5	0	8	50	<LOQ
B*	2.33 (2.37)	2.57 (2.38)	<LOD	<LOD	>25	>25	8	113	55

no evidence for typical disinfection by-products (Fig. S6) like trihalo-methanes, haloacetic acids or halogenated  $\alpha$ -hydroxycarboxylic acids [86,91] – so equations (A12) and (A13) (Table 2) can be ruled out.

In halide-ion containing electrolytes, reactive halogene species (RX) with high disinfecting potential are formed at the anode (Table 3). The formation of RX is depending on electrode surface properties and electrolysis parameters [30]. Therefore we investigated catholyte and anolyte of KI electrolytes with/without LA after different durations of electrolysis at 7 V, 300 mA, with the so-called DPD method [92]. From the results (Fig. 4) four conclusions were drawn: i) RX formed only at the anode, ii) with increasing electrolysis duration the amount of formed RX increased with saturation behavior, iii) the formation kinetics were found to be dependent on electrolyte concentration, iv) when LA was present, the formation of RX was accelerated in the first 60 s, thereafter the final RX concentrations were almost at the same level.

To quantify the amount of formed iodine, spectrophotometry in the UV/vis wavelength regime was used (Fig. S7). From Fig. 4 it was evident that the iodine concentration at the anode increased with electrolysis time and reacts with iodide to form triiodide which absorbs UV irradiation at 287 nm and 352 nm [93,94]. The later wavelength can be used to determine the amount of generated iodine (Table 3). UV spectra revealed that if LA was present the solution formed triiodide immediately when exposed to sunlight (data not shown; solution got more yellowish over time), even without electrolysis and the amount of generated  $\text{I}_3^-$  was reduced in the presence of LA. The first phenomenon was attributed to the better solubility of  $\text{I}_2/\text{I}_3^-$  in organic than in aqueous phases [95]. The later one suggested immediate reactions of formed iodine with

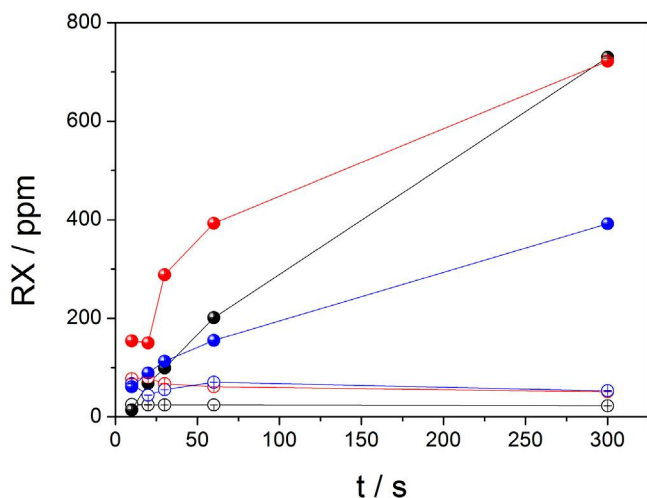


**Fig. 4.** Determined RX concentrations via DPD photometry at different electrolysis times; concentration at anode (full spheres), cathode (empty circles); conditions: cell type “HorSep”, Ti-cathode, Pt-anode, 7 V, 300 mA, 37 °C, solutions: A (black), A\* (red), B\* (blue). (For interpretation of the references to color in this figure legend, the reader is referred to the web version of this article.)

LA. The amount of formed iodine by electrolysis increased linearly with the concentration of iodide in the used electrolyte.

Overall as no ozone, hydroxyl radicals and hydrogen peroxide were detected at the cathode and the CV clearly showed the ORR, the main reactions taking place at the cathode were identified as (C1)–(C3) – main reactions being the HER and the ORR occurring probably through a “4 e<sup>−</sup> pathway” [54]. On the anode side a massive iodine/triiodide formation was observed and minor quantities of iodate and hydrogen peroxide were found. This indicates that reactions (A2)–(A5), (A8) and (A10) take place to some extent. For the given cell and electrode geometries the overpotential for the oxygen evolution reaction A1 was too large, and no oxygen formation was observed. In the case of LA addition no changes after electrolysis in terms of concentration were determined, rendering (A12) and (A13) unlikely.

The analysis of electrolysis products revealed as major products iodine/triiodide, hydrogen (which leaves the system as gaseous compound), hydroxide ions (for the unbuffered cases) and hydrogen peroxide. In the next step, the viability of *E. coli* biofilms grown on titanium surface was tested against the used electrolytes before and after electrolysis and against synthetic solutions containing the endpoint concentrations of the quantified active substances (Fig. 5).

Viability was tested by incubation of the biofilms for 12 h in the test solution, followed by the LIVE/DEAD™ assay with a fluorescence microscope; extreme cases are exemplified in Fig. 5a–c. For the native electrolytes A, A\*, B and B\* no significant killing activity was observed which was also true for phosphate buffer solutions with varying pH value (2, 6, 7.6, 11) and LA solutions (63 mM, 32 mM). Treatment with PBS solutions as well as the LA and concentrated iodate solutions resulted in a detachment of bacteria within the test period (Fig. 5d). Hydrogen peroxide and Lugol’s iodine killed many bacteria, but the incubation time was too short to have a significant effect. When electrolyzed anolytic and catholytic solutions of the electrolytes A, A\*, B and B\* were tested (Fig. 5e–f), i) the anodically formed species killed significantly more bacteria than the cathodic products, ii) the bactericidal effect increased with increasing electrolysis voltage, iii) bacterial detachment was observed for both, catholyte and anolyte, solutions. No clear correlation of the ionic strength of the electrolytes with the efficacy of the solutions was observed. The relatively high amount of dead microorganisms in electrolyzed anolyte/catholyte solutions suggested that further reactive, oxidative species such as hydroxyl radicals might be present.

### 3.5. Electrochemical removal of *E. coli* biofilms from titanium surfaces and dental implants

Oral implants are at risk of becoming colonized by biofilms that cause inflammation of their supporting tissues. Failing implants are associated with microbial colonization. To model these, biofilms were grown from *E. coli* overnight cultures (OD<sub>600</sub> 0.5) in LB medium on all electrode types at 37 °C while shaking at 100 rpm for 24 h. The generated films were quite stable and could be prepared [96] for SEM and AFM to investigate the morphology and size of the bacteria on the titanium substrates (Fig. S8). The general dimensions of single, non-corrupted *E. coli* bacteria were found to be: length 1.5–2  $\mu\text{m}$ , width 1–1.5  $\mu\text{m}$ , height 400–550 nm – which was consistent with published values [97]. The removal of these biofilms by the electrochemical approach was monitored by IRRAS, high-speed video analysis and fluorescence microscopy.

As mentioned in Chapter 3.2, flat titanium surfaces with native oxide layers are very well suited for IRRAS studies. Indeed, when *E. coli* biofilms were grown on titanium surfaces, bands characteristic for cellular and extracellular matrix components [98,99] became visible (Fig. 6, red). Of these, the 3297  $\text{cm}^{-1}$  band was attributed to adenine, cytosine and H-bonded OH groups. The three bands at 1662, 1542 and 1243  $\text{cm}^{-1}$ , respectively, can be assigned to amide vibrations and are related to cell proteins and  $\alpha$ -helical and  $\beta$ -pleated sheet structures, which absorb most efficiently at 1655–1637  $\text{cm}^{-1}$  [95,96]. The



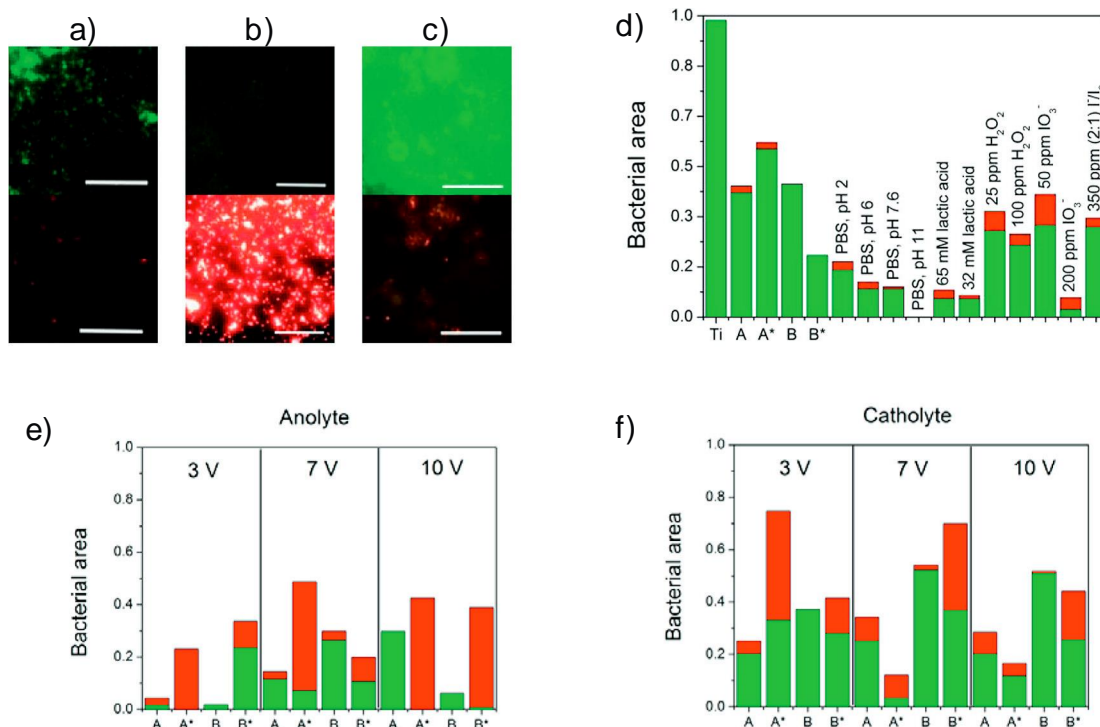


**Fig. 5.** a)–c) Fluorescence microscopy images of viability assay of *E. coli* biofilms with blind test solutions (upper row: viable bacteria [green], lower row: dead bacteria [red]), scale bar: 50  $\mu$ m; a) *E. coli* biofilm on bare Ti substrates, b) *E. coli* biofilm on Ti after 12 h treatment with electrolyzed A\* anolyte, c) *E. coli* biofilm on Ti after 12 h treatment with electrolyzed B catholyte; d–f) Cell viability fraction of bacterial biofilm measured from LIVE/DEAD™ assay after treatment for 12 h with blind test solutions, viable bacteria (green), dead bacteria (red), e) after 12 h treatment with anolytes obtained after electrolysis of various electrolytes at 3 V (left), 7 V (middle) and 10 V (right), f) after 12 h treatment with catholytes obtained after electrolysis of various electrolytes at 3 V (left), 7 V (middle) and 10 V (right). All electrolyses were carried out at 37 °C in cell type “HorSep”. (For interpretation of the references to color in this figure legend, the reader is referred to the web version of this article.)

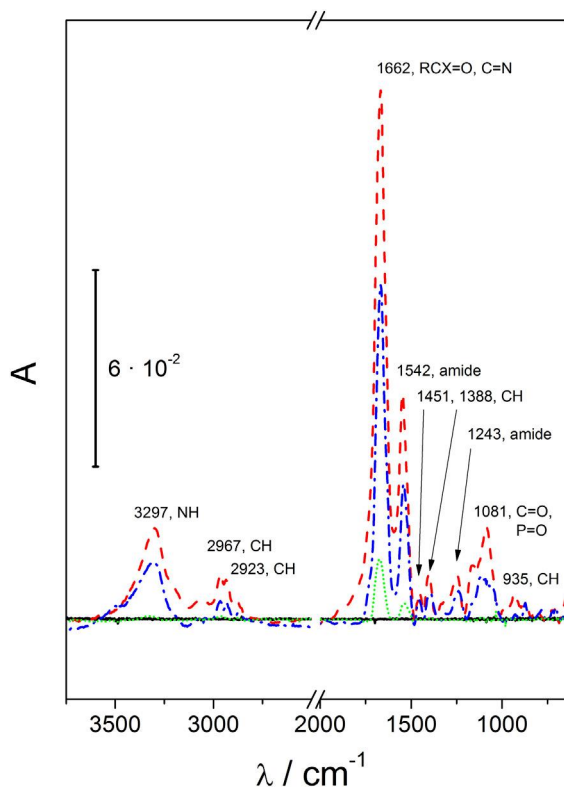


**Fig. 6.** IRRA spectra of bare titanium (black) and *E. coli* biofilms on Ti substrates; before (red, dashed) and after 30 s of electrolysis in A\* at 3 V (blue, dotted-dashed) and 7 V (green, dotted). Background was a plain titanium substrate. Band assignment can be found in supporting information (Table S1). (For interpretation of the references to color in this figure legend, the reader is referred to the web version of this article.)

stretching and bending vibrations of  $\text{CH}_2$  and  $\text{CH}_3$  of fatty acids and carbohydrates [95,96] were found at  $2967 \text{ cm}^{-1}$ ,  $2923 \text{ cm}^{-1}$ ,  $1451 \text{ cm}^{-1}$  and  $1388 \text{ cm}^{-1}$ , respectively. Glycopeptidic carbonyl groups and  $\text{P=O}$  stretching were responsible for the strong signal at  $1081 \text{ cm}^{-1}$  [95,96]. When the samples were electrolyzed for 30 s in solution A\*, the corresponding bands were reduced successively with increased electrolysis cell voltage which related well to the observation of macroscopic removal of the biofilms (Fig. 6).

Furthermore the success of removal of as-grown *E. coli* biofilms was tested by LIVE/DEAD™ assay (Figs. S9–S12). For low cell voltages and an electrolysis time of 30 s, a huge difference between electrolytes with/without LA was obvious. In A the amount of viable cells decreased with open cell voltage and viable bacteria were reduced by one order of magnitude at 7 V (Fig. 7a and d). In solution A\* an increased detachment of biofilms was observed at lower cell voltages as for solution A and the total reduction at 7 V and 10 V cell voltage was two orders of magnitude (Fig. 7b and e). We also studied the effect of electrolysis time at 7 V, 300 mA and observed a complete disinfection (reduction of viable bacteria by 5 orders of magnitude) after 60 s and that prolonging the electrolysis did not reduce the number of viable bacteria significantly (Fig. 7c and f). The electrolysis was also possible with different hydroxycarboxylic acids, but not as efficient as with LA (data not shown).

Finally the successful removal of mature wild type, multi-species biofilms from a titanium dental implant was studied by video analysis (Fig. 8). For the growth of the biofilm, ten saliva samples (5 male, 5 female test subjects) were combined, cultivated and then grown onto the substrates at 37 °C for 14 days. A Straumann type dental implant screw, overgrown by such a multi-species biofilm is shown in the first image of Fig. 8. The red circle in this image signifies a particular large chunk located in the trench of the thread. The electrolysis was then filmed with 240 frames per second and the respective images show the efficient removal of biofilm fragments by hydrogen evolution at the titanium cathode. Due to the high-speed filming conditions, the

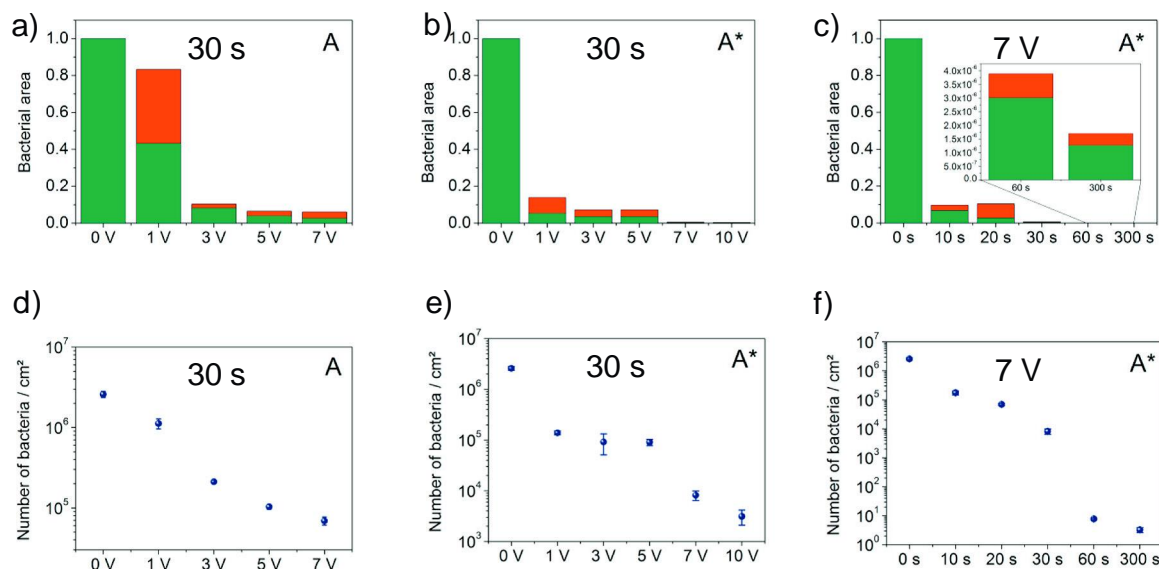


**Fig. 7.** a)–c): Cell viability fraction of bacterial biofilm on Ti substrates measured from LIVE/DEAD assay after electrolysis in different electrolytes and at various voltages and electrolysis times, viable bacteria (green), dead bacteria (red); d)–f): Counted bacteria per cm<sup>2</sup> on Ti substrates corresponding to a)–c). (For interpretation of the references to color in this figure legend, the reader is referred to the web version of this article.)

fate of the chunk could be followed in detail. At the end of the procedure, the implant remains completely clean (Fig. 8, last image).

#### 4. Conclusions

In this study, we could show that the electrochemical cleaning and disinfection of titanium surfaces is viable, if suitable conditions, such as electrode potentials and electrolyte compositions, are optimized. To study the involved phenomena and chemical species, different model electrodes and electrochemical set-ups were employed.

The electrochemical reactions at titanium electrodes were investigated by CV and OCP measurements at resting and electrolysis potential. There exist two competing reactions, namely the ORR ( $-1.0 \text{ V} < E < -0.5 \text{ V}$ ) and the HER ( $E < -1.4 \text{ V}$ ) of which the later dominates at lower potentials. The ORR reduces the local oxygen supply which might lead to a drastic reduction of aerobic bacteria, though the majority of biofilms was removed mechanically by the hydrogen bubbles generated at the cathode during electrolysis. Analyses of the composition of the electrolytes before and after electrolysis showed that the main products at the cathode were hydrogen and hydroxide ions, while the formation of ozone or hydrogen peroxide was not observed. Iodine in the form of triiodide and hydrogen peroxide were the major components formed at the anode. The solution's pH was stabilized, the iodine formation accelerated and the ORR shifted to more anodic potentials (while the HER potential was lowered) when lactic acid was present in the electrolyte.

Blind testing of the bactericidal effect of the found electrolysis product revealed that iodine and hydrogen peroxide were the main disinfectants. Therefore the efficacy of solutions containing lactic acid was reached at lower cell voltages compared to electrolytes without lactic acid. Lactic acid did not show bactericidal effects on its own.

With this knowledge at hand, *E. coli* biofilms were grown onto model titanium electrodes for two days, and then polarized cathodically in iodide-containing electrolytes and the residual fraction of adherent bacteria quantified by IRRAS and fluorescence microscopy. If the polarization potential was  $-0.5$  or  $-1.0 \text{ V}$  (vs.  $\text{Ag}/\text{Ag}^+$ ) the viable bacteria were reduced drastically though the disinfection was incomplete. The efficiency of the biofilm removal from titanium surfaces was significantly improved by decreasing the potential  $E < -1.4 \text{ V}$  (vs.  $\text{Ag}/\text{Ag}^+$ ), by using a buffered solution with  $\alpha$ -hydroxycarboxylic acids (mainly lactic acid) and by elongation of the electrolysis time. The final electrolysis parameters of 30 s at 7.0 V and 300 mA were sufficient to remove successfully 14-day old wildtype biofilms from dental implants *in vitro*.

#### Acknowledgement

The authors thank M. Füsler (University Frankfurt) for GC-MS measurements, GalvoSurge AG (Switzerland) for funding and fabrication of SLA type disc electrodes. The authors also thank H. Zipprich and C. Ratka for the provision of the titanium dental implants with/without mature wild type, multi-species biofilms.

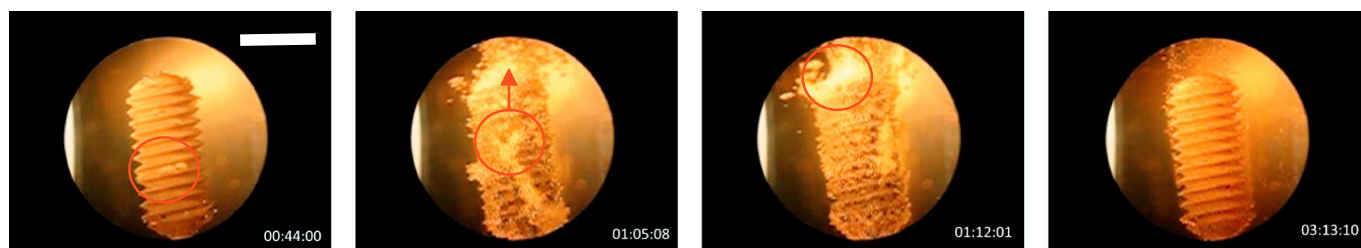


**Fig. 8.** Selected images of the electrochemical removal of a mature wild type biofilm from a titanium cathode (Straumann SLA implant) in solution A\*, 7 V/300 mA. First image shows electrode with biofilm before electrolysis, last image shows electrode after electrolysis. Scale bar: 4 mm. A red circle indicates the removal of a macroscopic chunk of biofilm. More images can be found in Fig. S13. (For interpretation of the references to color in this figure legend, the reader is referred to the web version of this article.)

## Appendix A. Supplementary data

Supplementary data to this article can be found online at <https://doi.org/10.1016/j.bioelechem.2018.01.008>.

## References

- [1] H. Algraffee, F. Borumandi, L. Cascarini, Peri-implantitis, *Br. J. Oral Maxillofac. Surg.* 50 (2012) 689–694.
- [2] Stefan Renvert, Anne Marie Roos-Jansåker, Christel Lindahl, Helena Renvert, G. Rutger Persson, Infection at titanium implants with or without a clinical diagnosis of inflammation, *Clin. Oral Implants Res.* 18 (2007) 509–516.
- [3] N.U. Zitzmann, T. Berglundh, Definition and prevalence of peri-implant diseases, *J. Clin. Periodontol.* 35 (2008) 286–291.
- [4] A. Mombelli, N.P. Lang, The diagnosis and treatment of peri-implantitis, *Periodontol.* 17 (2000) 63–76.
- [5] F. Schwarz, A. Schmucker, J. Becker, Efficacy of alternative or adjunctive measures to conventional treatment of peri-implant mucositis and peri-implantitis: a systematic review and meta-analysis, *Int. J. Implant Dentistry* 1 (2015) 1–34.
- [6] Aifang Han, James K.H. Tsoi, Flávia Pires Rodrigues, Julian G. Leprince, William M. Palin, Bacterial adhesion mechanisms on dental implant surfaces and the influencing factors, *Int. J. Adhes. Adhes.* 69 (2016) 58–71.
- [7] A. Mombelli, Microbiology and antimicrobial therapy of peri-implantitis, *Periodontol.* 28 (2000) 177–189.
- [8] U. Brodbeck, M. Schlee, H. Zipprich, Treatment System for Cleaning a Component, in Particular an Implant Part, Contaminated With a Biofilm, German Patent, WO2014/122188A1, 14.08.2014.
- [9] M. Schlee, U. Brodbeck, H. Zipprich, Treatment Liquid for Cleaning an Implant Part, German Patent, WO2014/122187A1, 14.08.2014.
- [10] U. Brodbeck, M. Schlee, H. Zipprich, Treatment Element for Treatment System for Dental Implant Component, Comprises Base Body, Which has Conductor Element and Connection System for Mechanical Connection With Dental Implant Component and is Provided With Medium Channel, German Patent, DE10201202593B3, 13.03.2014.
- [11] D. Mohn, M. Zehnder, W.J. Stark, T. Imfeld, Electrochemical disinfection of dental implants – a proof of concept, *PLoS One* 6 (2011), e16157.
- [12] P. Sahrman, M. Zehnder, D. Mohn, A. Meier, T. Imfeld, T. Thurnheer, Effect of low direct current on anaerobic multispecies biofilm adhering to a titanium implant surface, *Clin. Implant. Dent. Relat. Res.* 16 (2014) 552–556.
- [13] E.L. Sandvik, B.R. McLeod, A.E. Parker, P.S. Stewart, Direct electric current treatment under physiologic saline conditions kills *Staphylococcus epidermidis* biofilms via electrolytic generation of hypochlorous acid, *PLoS One* 8 (2013), e55118.
- [14] R. Gargi, V. Harshad, P. Mukesh, R. Jadhav, Efficacy of some antiseptics and disinfectants: a review, *Int. J. Pharmacy Pharm. Res.* 4 (2015) 182–197.
- [15] P. Maris, Modes of action of disinfectants, *Rev. Sci. Tech. OIE* 14 (1995) 47–55.
- [16] S. Sennhenn-Kirchner, J. Schliesing, H.G. Jacobs, H. Mergeryan, Antimikrobielle Wirkung verschiedener chemischer Agenzien auf rauen Titanoberflächen, *Z. Zahnärztl. Impl.* 20 (2004) 152–157.
- [17] B. Guggenheim, A. Meier, Die In-vitro-Wirkung von Chlorhexidin enthaltenden Mundspüllösungen auf Polyspezies-Biofilme, Schweiz. Monatsschr. Zahnmed. 121 (2011) 437–441.
- [18] M. Gosau, S. Hahnel, F. Schwarz, T. Gerlach, T.E. Reichert, R. Bürgers, Effect of six different peri-implantitis disinfection methods on *in vivo* human oral biofilm, *Clin. Oral Implants Res.* 21 (2010) 866–872.
- [19] A. Molander, C. Reit, G. Dahlen, The antimicrobial effect of calcium hydroxide in root canals pretreated with 5% iodine potassium iodide, *Endod. Dent. Traumatol.* 15 (1999) 205–209.
- [20] J. Tello-Barbaran, H.M. Nakata, D. Salcedo-Moncada, C.M. Bramante, R. Ordinola-Zapata, The antimicrobial effect of iodine-potassium iodide after cleaning and shaping procedures in mesial root canals of mandibular molars, *Acta Odontol. Latinoam.* 23 (2010) 244–247.
- [21] M. Haapasalo, E. Siren, D. Orstavik, T. Waltimo, Compositions and Method for the Disinfection of Dental Root Canals, Finish Patent, WO00/53150, 10.03.2000.
- [22] Eva Siren, Markus P.P. Haapasalo, Tuomas M.T. Waltimo, Dag Orstavik, *In vitro* antibacterial effect of calcium hydroxide combined with chlorhexidine or iodine potassium iodide on *Enterococcus faecalis*, *Eur. J. Oral Sci.* 112 (2004) 326–331.
- [23] N. Brändle, M. Zehnder, R. Weiger, T. Waltimo, Impact of growth conditions on susceptibility of five microbial species to alkaline stress, *J. Endod.* 34 (2008) 579–582.
- [24] M.R. Parini, W.G. Pitt, Dynamic removal of oral biofilms by bubbles, *Colloids Surf. B* 52 (2006) 39–46.
- [25] P. Sahrman, V. Ronay, D. Hofer, T. Attin, R.E. Jung, P.R. Schmidlin, *In vitro* cleaning potential of three different implant debridement methods, *Clin. Oral Implants Res.* (2013) 1–6.
- [26] R. Mengel, C. Meer, L. Flores-de-Jacoby, The treatment of uncoated and the treatment of uncoated and titanium nitride-coated abutments with different instruments, *Int. J. Oral Maxillofac. Implants* 19 (2004) 232–238.
- [27] Z. Wang, Y. Shen, J. Ma, M. Haapasalo, The effect of detergents on the antibacterial activity of disinfecting solutions in dentin, *J. Endod.* 38 (2012) 948–953.
- [28] C.P. Davis, M.E. Shirliff, N.M. Trieff, S.L. Hoskins, M.M. Warren, Quantification, qualification, and microbial killing efficiencies of antimicrobial chlorine-based substances produced by iontophoresis, *Antimicrob. Agents Chemother.* 38 (1994) 2768–2774.
- [29] G. Patermarakis, E. Fountoukidis, Disinfection of water by electrochemical treatment, *Water Res.* 24 (1990) 1491–1496.
- [30] J. Jeong, C. Kim, J. Yoon, The effect of electrode material on the generation of oxidants and microbial inactivation in the electrochemical disinfection processes, *Water Res.* 43 (2009) 895–901.
- [31] C.A. Martinez-Huitle, E. Brillas, Electrochemical alternatives for drinking water disinfection, *Angew. Chem. Int. Ed.* 47 (2008) 1998–2005.
- [32] C. Rabinovitch, P.S. Stewart, Removal and inactivation of *Staphylococcus epidermidis* biofilms by electrolysis, *Appl. Environ. Microbiol.* 72 (2006) 6364–6366.
- [33] Ozlem Istanbulu, Jerome Babauta, Hung Duc Nguyen, Haluk Beyenal, Electrochemical biofilm control: mechanism of action, *Biofouling* 28 (2012) 769–778.
- [34] M.T. Ehrensberger, M.E. Tobias, S.R. Nodzo, L.A. Hansen, N.R. Luke-Marshall, R.F. Cole, L.M. Wild, A.A. Campagnari, Cathodic voltage-controlled electrical stimulation of titanium implants as treatment for methicillin-resistant *Staphylococcus aureus* periprosthetic infections, *Biomaterials* 41 (2015) 97–105.
- [35] S.H. Hong, J. Jeong, S. Shim, H. Kang, S. Kwon, K.H. Ahn, J. Yoon, Effect of electric currents on bacterial detachment, and inactivation, *Biotechnol. Bioeng.* 100 (2008) 379–386.
- [36] M. Dargahi, Z. Hosseinioust, N. Tufenkji, S. Omanovic, Investigating electrochemical removal of bacterial biofilms from stainless steel substrates, *Colloids Surf. B* 117 (2014) 152–157.
- [37] Philipp Sahrman, Dirk Mohn, Matthias Zehnder, Wendelin Stark, Thomas Imfeld, Franz Weber, Effect of direct current on surface structure and cytocompatibility of titanium dental implants, *Int. J. Oral Maxillofac. Implants* 29 (2014) 735–742.
- [38] W.K. Liu, M.R. Brown, T.S. Elliott, Mechanisms of the bactericidal activity of low amperage electric current (DC), *J. Antimicrob. Chemother.* 39 (1997) 687–695.
- [39] M.T. Ehrensberger, S. Sivan, J.L. Gilbert, Titanium is not “the most biocompatible metal” under cathodic potential: the relationship between voltage and MC3T3 preosteoblast behavior on electrically polarized cpTi surfaces, *J. Biomed. Mater. Res. A* 93A (2009) 1500–1509.
- [40] M.T. Ehrensberger, J.L. Gilbert, The effect of scanning electrochemical potential on the short-term impedance of commercially pure titanium in simulated biological conditions, *J. Biomed. Mater. Res. A* 94A (2010) 781–789.
- [41] B.G. Pound, Passive films on metallic biomaterials under simulated physiological conditions, *J. Biomed. Mater. Res. A* 102A (2014) 1595–1604.
- [42] M.T. Ehrensberger, J.L. Gilbert, The effect of static applied potential on the 24-hour impedance behavior of commercially pure titanium in simulated biological conditions, *J. Biomed. Mater. Res. B* 93B (2010) 106–112.
- [43] E. Brooks, M. Tobias, K. Krautsak, M. Ehrensberger, The influence of cathodic polarization and simulated inflammation on titanium electrochemistry, *J. Biomed. Mater. Res. B* 102B (2014) 1445–1463.
- [44] J. Park, P. Du, J.-K. Jeon, G. Hyuk Jang, M.P. Hwang, H.-S. Han, K. Park, K.H. Lee, J.-W. Lee, H. Jeon, Y.-C. Kim, J.W. Park, H.-K. Seok, M.-R. Ok, Magnesium corrosion triggered spontaneous generation of H<sub>2</sub>O<sub>2</sub> on oxidized titanium for promoting angiogenesis, *Angew. Chem. Int. Ed.* 54 (2015) 14753–14757.
- [45] M. Kalbacova, S. Roessler, U. Hempel, R. Tsaryk, K. Peters, D. Scharnweber, J.C. Kirkpatrick, P. Dieter, The effect of electrochemically simulated titanium cathodic corrosion products on ROS production and metabolic activity of osteoblasts and monocytes/macrophages, *Biomaterials* 28 (2007) 3263–3272.
- [46] J.L. Del Pozo, M.S. Rouse, R. Patel, Bioelectric effect and bacterial biofilms. A systematic review, *Int. J. Artif. Organs* 31 (2008) 786–795.
- [47] J.W. Costerton, B. Ellis, K. Lam, F. Johnson, A.E. Khoury, Mechanism of electrical enhancement of efficacy of antibiotics in killing biofilm bacteria, *Antimicrob. Agents Chemother.* 38 (1994) 2803–2809.
- [48] S.A. Blenkinsopp, A.E. Khoury, J.W. Costerton, Electrical enhancement of biocide efficacy against *Pseudomonas aeruginosa* biofilms, *Appl. Environ. Microbiol.* 58 (1992) 3770–3773.
- [49] H. Wang, D. Ren, Controlling *Streptococcus mutans* and *Staphylococcus aureus* biofilms with direct current and chlorhexidine, *AMB Express* 7 (2017) 204.
- [50] T.H.R. Niepa, L.M. Snepenger, H. Wang, S. Sivan, J.L. Gilbert, M.B. Jones, D. Ren, Sensitizing *Pseudomonas aeruginosa* to antibiotics by electrochemical disruption of membrane functions, *Biomaterials* 74 (2016) 267–279.
- [51] D. Andes, J. Nett, P. Oschel, R. Albrecht, K. Marchillo, A. Pitula, Development and characterization of an *in vivo* central venous catheter *Candida albicans* biofilm model, *Infect. Immun.* 72 (2004) 6023–6031.
- [52] J. Messing, R. Crea, P.H. Seeburg, A system for shotgun DNA sequencing, *Nucleic Acids Res.* 9 (1981) 309–321.
- [53] M. Hartmann, A.K. Horst, P. Klemm, T.K. Lindhorst, A kit for the investigation of live *Escherichia coli* cell adhesion to glycosylated surfaces, *Chem. Commun.* 46 (2010) 330–332.
- [54] G. Bertani, Studies on lysogenesis I. The mode of phage liberation by lysogenic *Escherichia coli*, *J. Bacteriol.* 62 (1951) 293–300.
- [55] J. Schindelin, I. Arganda-Carreras, E. Frise, V. Kaynig, M. Longair, T. Pietzsch, S. Preibisch, C. Rueden, S. Saalfeld, B. Schmid, J.-Y. Tinevez, D.J. White, V. Hartenstein, K. Eliceiri, P. Tomancak, A. Cardona, Fiji: an open-source platform for biological-image analysis, *Nat. Methods* 9 (2012) 676–682.
- [56] S.V. Mentus, Oxygen reduction on anodically formed titanium dioxide, *Electrochim. Acta* 50 (2004) 27–32.
- [57] Z. Wang, H. Deng, L. Chen, Y. Xiao, F. Zhao, *In situ* measurements of dissolved oxygen, pH and redox potential of biocathode microenvironments using microelectrodes, *Bioresour. Technol.* 132 (2013) 387–390.
- [58] B. Rebarry, P. Paul, P.K. Ghosh, Determination of iodide and iodate in edible salt by ion chromatography with integrated amperometric detection, *Food Chem.* 123 (2010) 529–534.
- [59] A. Becalski, B.P.-Y. Lau, T.J. Schrader, S.W. Seaman, W.F. Sun, Formation of iodoacetic acids during cooking: interaction of iodized table salt with chlorinated drinking water, *Food Addit. Contam.* 23 (2006) 957–962.



- [60] I. Katsounaros, W.B. Schneider, J.C. Meier, U. Benedikt, P.U. Biedermann, A.A. Auer, K. J.J. Mayrhofer, Hydrogen peroxide electrochemistry on platinum: towards understanding the oxygen reduction reaction mechanism, *PCCP* 14 (2012) 7384–7391.
- [61] R.O. Rahn, Determination of iodide formed from inorganic iodine in aqueous solution, *Anal. Chim. Acta* 248 (1991) 595–602.
- [62] R.C. Fuson, B.A. Bull, The haloform reaction, *Chem. Rev.* 15 (1934) 275–309.
- [63] K. Ramalinga, P. Vijayalakshmi, T.N.B. Kaimal, A mild and efficient method for esterification and transesterification catalyzed by iodine, *Tetrahedron Lett.* 43 (2002) 879–882.
- [64] B.K. Banik, M. Chapa, J. Marquez, M. Cardona, A remarkable iodine-catalyzed protection of carbonyl compounds, *Tetrahedron Lett.* 46 (2005) 2341–2343.
- [65] A.K. Banerjee, W. Vera, H. Mora, M.S. Laya, L. Bedoya, E.V. Cabrera, Iodine in organic synthesis, *J. Sci. Ind. Res.* 65 (2006) 299–308.
- [66] I. Zawisza, M. Nullmeier, S.E. Pust, R. Boukherroub, S. Szunerits, G. Wittstock, Application of thin titanium/titanium oxide layers deposited on gold for infrared reflection absorption spectroscopy: structural studies of lipid bilayers, *Langmuir* 24 (2008) 7378–7387.
- [67] F. Song, H. Koo, D. Ren, Effects of material properties on bacterial adhesion and biofilm formation, *J. Dent. Res.* 94 (2015) 1027–1034.
- [68] R.P. Cooney, P.J. Hendra, M. Fleischmann, Raman spectra from adsorbed iodine species on an unroughened platinum electrode surface, *J. Raman Spectrosc.* 6 (1977) 264–266.
- [69] H. Baltruschat, U. Bringemeier, R. Vogel, Scanning tunnelling microscopic investigation of iodine-covered Pt single-crystal electrodes, *Faraday Discuss.* 94 (1992) 317–327.
- [70] W.L. DeSimone, J.J. Breen, Structures of iodine on Pt(110) single crystal electrode surfaces, *Langmuir* 11 (1995) 4428–4432.
- [71] C.A. Lucas, N.M. Markovic, P.N. Ross, Adsorption of halide anions at the Pt(111)-solution interface studied by *in situ* surface x-ray scattering, *Phys. Rev. B* 55 (1997) 7964–7971.
- [72] R.M. Torresi, O.R. Camara, C.P. De Pauli, M.C. Giordano, Hydrogen evolution reaction on anodic titanium oxide films, *Electrochim. Acta* 32 (1987) 1291–1301.
- [73] R.M. Torresi, O.R. Camara, C.P. De Pauli, Influence of the hydrogen evolution reaction on the anodic titanium oxide film properties, *Electrochim. Acta* 32 (1987) 1357–1363.
- [74] Weiqiang Yu, Jing Qiu, Ling Xu, Fuqiang Zhang, Corrosion behaviors of TiO<sub>2</sub> nanotube layers on titanium in Hank's solution, *Biomed. Mater.* 4 (2009), 065012.
- [75] L. Kavan, Electrochemistry of titanium dioxide: some aspects and highlights, *Chem. Rec.* 12 (2012) 131–142.
- [76] M. Dolata, P. Kedzierzawski, J. Augustynski, Comparative impedance spectroscopy study of rutile and anatase TiO<sub>2</sub> film electrodes, *Electrochim. Acta* 41 (1996) 1287–1293.
- [77] K. Venkateswarlu, N. Rameshbabu, D. Sreekanth, M. Sandhyarani, A.C. Bose, V. Muthupandhi, S. Subramanian, Role of electrolyte chemistry on electronic and *in vitro* electrochemical properties of micro-arc oxidized titania films on CpTi, *Electrochim. Acta* 105 (2013) 468–480.
- [78] M.A. Ghanem, A.M. Al-Mayouf, M.N. Shaddad, F. Marken, Selective formation of hydrogen peroxide by oxygen reduction on TiO<sub>2</sub> nanotubes in alkaline media, *Electrochim. Acta* 124 (2015) 557–562.
- [79] S.V. Mentus, The evidence of limitation of oxygen reduction reaction by proton diffusion in low-concentration acid solutions, *J. Electroanal. Chem.* 738 (2015) 47–50.
- [80] D. Laser, M. Yaniv, S. Gottesfeld, Electrochemical and optical properties of thin oxide layers formed on fresh titanium surfaces in acid solutions, *J. Electrochem. Soc.* 125 (1978) 358–365.
- [81] Q. Qu, L. Wang, Y. Chen, L. Li, Y. He, Z. Ding, Corrosion behavior of titanium in artificial saliva by lactic acid, *Materials* 7 (2014) 5528–5542.
- [82] Alex E. Pozhitkov, Dianne Daubert, Ashley Brochewicz Donimirski, Douglas Goodgion, Mikhail Y. Vagin, Brian G. Leroux, Colby M. Hunter, Thomas F. Flemmig, Peter A. Noble, J.D. Byers, Interruption of electrical conductivity of titanium dental implants suggests a path towards elimination of corrosion, *PLoS One* 10 (2015), e0140393.
- [83] B. Parkinson, F. Decker, J.F. Juliao, M. Abramovich, H.C. Chagas, The reduction of molecular oxygen at single crystal rutile electrodes, *Electrochim. Acta* 25 (1980) 521–525.
- [84] T. Clark, D.C. Johnson, Activation of titanium electrodes for voltammetric detection of oxygen and hydrogen peroxide in alkaline media, *Electroanalysis* 9 (1997) 273–278.
- [85] P. Clechet, C. Martelet, J.R. Martin, R. Olier, Photoelectrochemical behaviour of TiO<sub>2</sub> and formation of hydrogen peroxide, *Electrochim. Acta* 24 (1997) 457–461.
- [86] F. Demir, A. Erdogmus, A. Koca, Oxygen reduction reaction catalyzed with titanyl phthalocyanines in nonaqueous and aqueous media, *PCCP* 15 (2013) 15926–15934.
- [87] H. Bader, J. Hoigné, Determination of ozone in water by the indigo method; a submitted standard method, *Ozone Sci. Eng.* 4 (1982) 169–176.
- [88] Y. Bichsel, U. von Gunten, Oxidation of iodide and hypiodous acid in the disinfection of natural waters, *Environ. Sci. Technol.* 33 (1999) 4040–4045.
- [89] Y. Bichsel, U. von Gunten, Hypiodous acid: kinetics of the buffer-catalyzed disproportionation, *Water Res.* 34 (2000) 3197–3203.
- [90] H. Bruchertseifer, R. Cripps, S. Guentay, B. Jaekel, Analysis of iodine species in aqueous solutions, *Anal. Bioanal. Chem.* 375 (2003) 1107–1110.
- [91] DIN EN ISO 7393-2, Water Quality — Determination of Free Chlorine and Total Chlorine - Part 2: Colorimetric Method Using N,N-diethyl-1,4-Phenylenediamine for Routine Control Purposes (ISO 7393-2: 1985), German Version EN ISO 7393-2, 2000.
- [92] J.J. Custer, S. Natelson, Spectrophotometric determination of microquantities of iodine, *Anal. Chem.* 21 (1949) 1005–1009.
- [93] L. Andrews, E.S. Prochaska, A. Loewenschuss, Resonance Raman and ultraviolet absorption spectra of the triiodide ion produced by alkali iodide-iodine argon matrix reactions, *Inorg. Chem.* 19 (1980) 463–465.
- [94] A.F. Holleman, N. Wiberg, *Lehrbuch der Anorganischen Chemie*, 101th edition De Gruyter, Berlin, 1995.
- [95] D. Andes, J. Nett, P. Oschel, R. Albrecht, K. Marchillo, A. Pitula, Development and characterization of an *in vivo* central venous catheter *Candida albicans* biofilm model, *Infect. Immun.* 72 (2004) 6023–6031.
- [96] J. Guo, Bacterial Biofilms on Electrochemically Active Cathodic Titanium Surfaces Master thesis Syracuse University, Syracuse, 2013.
- [97] D. Naumann, Infrared spectroscopy in microbiology, in: R.A. Meyers (Ed.), *Encyclopedia of Analytical Chemistry*, John Wiley & Sons Inc, Chichester, 2000.
- [98] F.S. Parker, *Applications of Infrared Spectroscopy in Biochemistry, Biology and Medicine*, Plenum Press, New York, 1971.



**Sebastian Schneider** is currently pursuing his Ph. D. in analytical chemistry under the supervision of Prof. Dr. Andreas Terfort. After several years in the chemical and pharmaceutical industry, he joined the Terfort group for electrochemical research. He holds a M. Sc. in Chemistry, a B. Sc. in Chemical Process Engineering and is a trained chemical laboratory assistant. His research is focused on microsenors, organic electronics and applied electrochemistry.



**Michael Rudolph** studied chemistry at the Goethe-University Frankfurt/Main (Germany). He prepared his B. Sc. thesis (Synthesis of new derivatives of the NDBF-protecting group to optimize the two-photon capture cross-section) in the group of Prof. Alexander Heckel and is currently pursuing his Master's degree in the group of Prof. Andreas Terfort, focusing on the development of analytical examination methods for halide-based disinfectants. He supervised numerous organic lab courses for biophysics students and participated in several industrial projects throughout his studies.



**Vanessa Bause** is currently finishing up her master thesis at the SGL Carbon Company (Meitingen, Germany) on the subject surface chemistry of carbon fiber based materials. Her technical focuses of the master degree are in analytical and surface chemistry. She holds a B. Sc. in chemistry and a B. Sc. in economics.



**Andreas Terfort** obtained his diploma in chemistry in Göttingen and his PhD in Regensburg. After a Post-Doc with G. M. Whitesides (Harvard University) he returned to Hamburg, where he completed his habilitation in 2003. He held different positions in Bochum, Frankfurt, Hamburg, Marburg before becoming a chair (Inorganic Chemistry) in Frankfurt. His research focusses on surface chemistry, including corrosion, bio-fouling, organic electronics, and sensing.